

1 **Attentional Modulations of Alpha Power Are Sensitive to the Task-relevance of Auditory** 2 **Spatial Information**

3 Laura-Isabelle Klatt, Stephan Getzmann, Daniel Schneider

4 *Leibniz Research Centre for Working Environment and Human Factors*

6 **Abstract**

7 The topographical distribution of oscillatory power in the alpha band is known to vary
8 depending on the current focus of spatial attention. Here, we investigated to what extent
9 univariate and multivariate measures of post-stimulus alpha power are sensitive to the
10 required spatial specificity of a task. To this end, we varied the perceptual load and the
11 spatial demand in an auditory search paradigm. A centrally presented sound at the
12 beginning of each trial indicated the to-be-localized target sound. This spatially unspecific
13 pre-cue was followed by a sound array, containing either two (low perceptual load) or four
14 (high perceptual load) simultaneously presented lateralized sound stimuli. In separate task
15 blocks, participants were instructed either to report whether the target was located on the
16 left or the right side of the sound array (low spatial demand) or to indicate the exact target
17 location (high spatial demand). Univariate alpha lateralization magnitude was neither
18 affected by perceptual load nor by spatial demand. However, an analysis of onset latencies
19 revealed that alpha lateralization emerged earlier in low (vs. high) perceptual load trials as
20 well as in low (vs. high) spatial demand trials. Moreover, across all conditions, participants
21 with earlier alpha lateralization onset showed faster response times. Finally, we trained a
22 classifier to decode the specific target location based on the multivariate alpha power scalp
23 topography. A comparison of decoding accuracy in the low and high spatial demand
24 conditions suggests that the amount of spatial information present in the scalp distribution
25 of alpha-band power increases as the task demands a higher degree of spatial specificity.
26 Altogether, the results offer new insights into how the dynamic adaption of alpha-band
27 oscillations in response to changing task demands is associated with post-stimulus
28 attentional processing.

29 *Keywords: alpha oscillations, EEG, multivariate pattern analysis, selective attention, spatial*
30 *specificity, sound localization*

1. Introduction

In everyday environments, containing multiple competing sensory inputs, focusing spatial attention on relevant information while ignoring or suppressing irrelevant information is crucial to engage in goal-directed behaviour. Consistently, covert shifts of spatial attention have been shown to improve various aspects of behavioural performance, including visual spatial acuity (reviewed by Anton-Erxleben & Carrasco, 2013), contrast sensitivity (Carrasco, Penpeci-Talgar, & Eckstein, 2000), or the rate of information accumulation (Carrasco & McElree, 2001). On the electrophysiological level, asymmetric modulations of parieto-occipital alpha-band power present a robust signature of spatial attentional orienting. Typically, alpha-band power decreases contralateral to the attended location and / or increases over ipsilateral scalp sites. This phenomenon of alpha power lateralization has been found in response to anticipatory shifts of attention (Foxe, Simpson, & Ahlfors, 1998; Worden, Foxe, Wang, & Simpson, 2000), when retro-actively attending to working memory representations (Poch, Capilla, Hinojosa, & Campo, 2017; Schneider, Mertes, & Wascher, 2016), as well as during post-stimulus attentional processing (e.g., in auditory or visual search paradigms; Bacigalupo & Luck, 2019; Klatt, Getzmann, Wascher, & Schneider, 2018b).

Accumulating evidence suggests that scalp-level alpha-band activity not only reflects the attended hemifield but is tuned specifically to the attended visual field location (Bahramisharif, Heskes, Jensen, & van Gerven, 2011; Rihs, Michel, & Thut, 2007). Moreover, this spatial selectivity is also reflected in the retinotopic organization of alpha sources (Popov, Gips, Kastner, & Jensen, 2019). First evidence for comparable ‘spatial tuning’ of alpha-band oscillations in the auditory domain comes from a recent study by Deng and colleagues (Deng, Choi, & Shinn-Cunningham, 2020) who found that the topographic distribution of posterior alpha-band lateralization changes monotonically as the focus of auditory spatial attention shifts in space.

Notably, recent evidence suggests that the degree of spatial specificity reflected in the scalp distribution of alpha-band power also depends on the current task demands (Feldmann-Wüstefeld & Awh, 2019; Voytek et al., 2017). Specifically, two studies of visual anticipatory spatial attention, using multivariate inverted encoding models (IEM), demonstrated that the spatial selectivity of alpha activity increased when participants voluntarily focused on a narrow rather than a broad region of space (Feldmann-Wüstefeld &

Awh, 2020) and scaled to the degree of certainty of a central cue that indicated the location of an upcoming target (Voytek et al. 2017).

Consistently, in an auditory spatial attention study, focusing on post-stimulus attentional processing, we found that task-demands shape the reliance on alpha-band mediated post-stimulus processing. That is, auditory post-stimulus alpha lateralization was only present in a spatially specific sound localization task, whereas it was absent in a simple sound detection paradigm (Klatt et al. 2018b, see also Deng et al. 2019). In the present study, we set out to further investigate to what extent attentional modulations of post-stimulus alpha power capture the spatial demands of a sound localization task on a more fine-grained scale. To this end, we varied both the perceptual load and the spatial demand of the task. That is, participants were asked to localize a target sound among a set of either two (low perceptual load) or four (high perceptual load) concurrently presented sounds in a lateralized sound array. In separate task blocks, they either indicated (a) whether the target was present on the left or the right side (i.e., two response options, low spatial demand) or (b) reported the exact target location (i.e., four response options, high spatial demand). On the behavioural level, we expected that high perceptual load (compared to low load) and high spatial demand (compared to low spatial demand) would present the more challenging listening situation, resulting in slower response times and lower sound localization accuracy. Beyond that, attempting to replicate previous results, we hypothesized that post-stimulus modulations of alpha-band power should index the attended target location, while the magnitude thereof should not be affected by perceptual load (Klatt et al., 2018b). This should be evident in a hemispheric lateralization of alpha-band power over parieto-occipital electrode sites in both low and high perceptual load trials.

Further, the critical aim of this study was to assess whether the required degree of behavioural spatial specificity (low vs. high spatial demand) affects the spatial specificity of the alpha power signal. If this is the case, this should be either evident in a modulation of alpha lateralization magnitude and / or captured by the scalp distribution of alpha-band power. Hence, we applied both univariate as well as multivariate analysis techniques to evaluate alpha-band power modulations depending on the spatial (and perceptual) demands of the task. Finally, we assessed alpha lateralization onset latencies to explore whether the time course of alpha-band activity is likewise modulated by the required degree of spatial specificity or perceptual load. Specifically, if slower sound localization performance in high

spatial demand or high perceptual load conditions coincides with slower post-stimulus attentional processing, this should be reflected in delayed onset latencies of alpha lateralization. Such a time-resolved modulation of attentional alpha-band activity is, for instance, suggested by Foster and colleagues (Foster, Sutterer, Serences, Vogel, & Awh, 2017), who showed that the onset latency of location-selective alpha-band channel tuning functions (reconstructed from the topographic distribution of alpha-band oscillatory power) occurred later in time for trials with slow compared to fast responses as well as for a hard compared to an easier search condition.

2. Methods

2.1 Ethics statement

The study was approved by the Ethical Committee of the Leibniz Research Centre for Working Environment and Human Factors and conducted in accordance with the Declaration of Helsinki. All participants provided written informed consent prior to the beginning of the experimental procedure.

2.2 Participants

19 participants were recruited to take part in the study. Hearing acuity was assessed using a pure-tone audiometry (Oscilla USB 330; Inmedico, Lystrup, Denmark), presenting eleven pure-tone frequencies in-between 125 Hz and 8000 Hz. One participant had to be excluded due to a unilateral, mild to moderate hearing impairment in the right ear (hearing thresholds of up to 35 – 50 dB hearing level). All other participants showed no signs of hearing impairment (hearing thresholds \leq 25 dB). Another participant did not correctly follow the task instructions and was also excluded. Thus, the final sample included 17 subjects (mean age 23.29 years, age range 19- 30, 9 female), all of which were right-handed as indicated by the Edinburgh Handedness Inventory (Oldfield, 1971). The sample size we aimed at was chosen to be comparable to previous publications from the lab that investigated similar electrophysiological measures (e.g., Klatt, Getzmann, Wascher, & Schneider, 2018b, 2018a). All participants had normal or corrected-to-normal vision, reported no history of or current neurological or psychiatric disorders and received course credit or financial compensation (10€/hour) for their participation.

2.2 Experimental setup and stimuli

The experiment was conducted in a dimly illuminated, anechoic, and sound-attenuated room ($5.0 \times 3.3 \times 2.4\text{m}^3$). Pyramid-shaped foam panels on ceiling and walls and a woolen carpet on the floor ensure a background noise level below 20dB(A). Participants were seated in a comfortable chair with their head position held constant by a chin rest. A semicircular array of nine loudspeakers (SC5.9; Visaton, Haan, Germany) was mounted in front of the subject at a distance of ~1.5 meters from the subject's head and at a height of ~1.3 meters (approximately at ear level). Only five loudspeakers, located at azimuthal positions of -90° , -30° , 0° , 30° , and 90° respectively, were used for the present experimental setup. A red, light-emitting diode (diameter 3 mm) was attached right below the central loudspeaker. The diode remained turned off during the experiment, but served as a central fixation target.

As sound stimuli, eight familiar animal vocalizations ('birds chirping', 'dog barking', 'frog croaking', 'sheep baaing', 'cat meowing', 'duck quacking', 'cow mooing', 'rooster crowing') were chosen from an online sound archive (Marcell, Borella, Greene, Kerr, & Rogers, 2000). The original sounds were cut to a constant duration of 600 ms (10 ms on/off ramp), while leaving the spectro-temporal characteristics unchanged. The overall sound pressure level of the sound arrays, containing either two or four concurrently present sounds, was about 63 dB(A) and 66 dB(A), respectively. The target sounds, presented in isolation from a central position, had a sound pressure level of 60 dB(A).

2.3 Procedure, task, and experimental design

The experiment consisted of an auditory search paradigm implementing a sound localization task. The sequence of events in a given trial is depicted in Figure 1. Each trial began with a silent period of 500 ms. Then a sound stimulus was presented from a central position (0° azimuth angle) for 600 ms, serving as a cue that indicated the to-be-localized target in a given trial. The latter was followed by a 1000 ms silent inter-stimulus-interval and the sound array (600 ms). The sound array contained either two (i.e., *low perceptual load*, 50%) or four (i.e., *high perceptual load*, 50%) simultaneously present lateralized sound stimuli. In low perceptual load trials, the sounds could occur at either of the four lateralized loudspeaker positions (-90° , -30° , 30° , 90° azimuth), with the restriction that the two sounds (i.e., the target and a non-target sound) were always present in different hemi-fields. Accordingly, in high perceptual load trials, in which the target sound was presented together with three

159 non-target sounds, all four lateralized active loudspeakers were used. In separate task
 160 blocks, participants either indicated whether the target sound was present on the left versus
 161 right side (i.e., *low spatial demand*, lsd) or indicated the exact target position (i.e., *high*
 162 *spatial demand*, hsd). In addition, both task blocks incorporated a proportion of target-
 163 absent trials that required no response. Target-absent trials were included to ensure that
 164 selectively listening to the input from only one side of the stimulus array presented no viable
 165 strategy in low spatial demand task blocks. That is, if the sound array always contained a
 166 target sound, subjects could be inclined to simply infer that the target was located on the
 167 left side solely because they didn't perceive it on the right side (or vice versa).

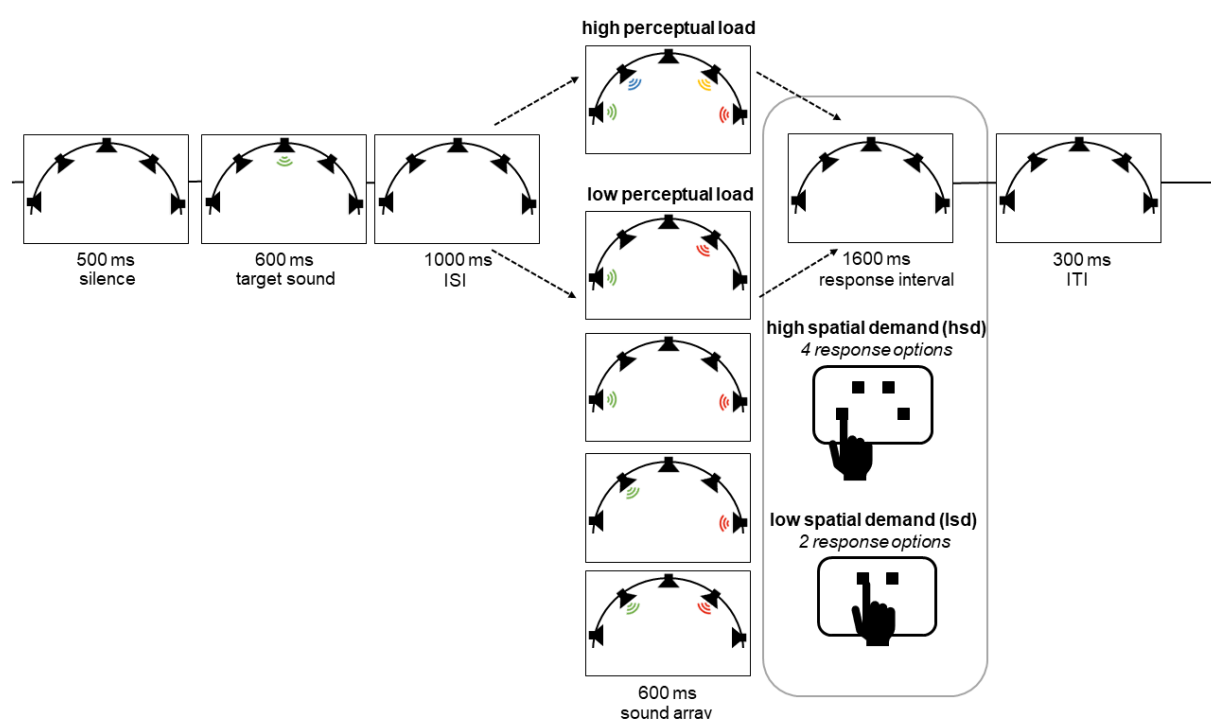


Figure 1. Schematic illustration of the experimental design. A centrally presented target cue indicated the relevant target in a given trial. Then, a sound array appeared, containing either two or four simultaneously present sounds from lateralized positions. In different task blocks, participants were asked to either indicate whether the target was presented on the left or the right side (low spatial demand) or to report the exact target location (high spatial demand). In both task blocks, it was also possible that the sound array did not contain the target (i.e., target-absent trial). In this case, participants withheld their response. ISI = inter-stimulus-interval, ITI = inter-trial-interval.

168 Sound array presentation was followed by a 1600 ms response interval and a 300 ms inter-
 169 trial-interval (ITI). In total, each trial lasted for 4600 ms (including the ITI). Participants
 170 indicated their response by pressing one out of four buttons, arranged in a semi-circular

array on a response pad. In high-spatial demand trials, each button corresponded to one of the loudspeaker positions, such that participants had to press the left-most button when the target was presented at the left-most loudspeaker, and so on. In low spatial demand trials, participants only used the two inner response buttons (i.e., the left button for left-target responses, the right button for right-target responses). Participants were instructed to always respond as accurately and as fast as possible, using the index finger of their right hand. To minimize horizontal eye movements during the EEG-recording, participants were instructed to fixate the central LED.

Each task block consisted of 672 trials, containing both low and high perceptual load trials in randomized order. Short, self-paced breaks after every 224 trials and in-between task blocks were conducted to prevent fatigue. The order of task blocks was counterbalanced across participants, such that $n = 8$ subjects first completed the low-spatial demand condition and $n = 9$ subjects first completed the high-spatial demand condition. Prior to the beginning of each task block, participants completed 40 practice trials to familiarize with the task. All participants were presented with the same semi-randomized selection of trials. Specifically, in both task blocks, the same selection of 672 trials was presented, but in a different, randomized order. This assured that all differences between conditions could be ascribed to the task manipulations rather than differences in the stimulus materials. Each of the eight animal vocalizations served as the target equally often (i.e., 84 times per block). In addition, the target sound appeared equally often at each of the four possible sound speaker locations (i.e., 56 times per location and perceptual load per block). This also ensured that the number of left (1/3) vs. right (1/3) responses in low-spatial demand trials as well as the number of outer-left (1/5), inner-left (1/5), inner-right (1/5), and outer-right (1/5) responses in high-spatial demand trials was counterbalanced across subjects. Target-absent trials constituted $1/3^{\text{rd}}$ and $1/5^{\text{th}}$ of all trials in low and high spatial demand task blocks, respectively. The timing of the stimuli was controlled by custom-written software. Participants did not receive feedback during the experiment.

Taken together, the present study comprised a 2×2 repeated-measures design, including the within-subject factors *spatial demand* (low vs. high spatial demand) and *perceptual load* (low vs. high perceptual load). Note that there are different ways of defining perceptual load (for a review see Murphy, Spence, & Dalton, 2017). Here, we refer to *perceptual load* as the number of items in the search display.

2.4 EEG data acquisition

The continuous EEG data were recorded from 58 Ag/AgCl passive scalp electrodes (ECI Electrocap, GVB-geliMED GmbH, Bad Segeberg, Germany) as well as from left and right mastoids. Electrode positions corresponded to the international 10-10 system. The electrooculogram (EOG) was simultaneously recorded from four additional electrodes, placed lateral to the outer canthus of each eye as well as below and above the right eye. The ground electrode was placed on the center of the forehead, right above the nasion. The average of all electrodes served as the online-reference. The data were recorded using a QuickAmp-72 amplifier (Brain products, Gilching, Germany) and digitized at a sampling rate of 1 kHz. During the preparation of the EEG cap, all electrode impedances were kept below 10 k Ω .

2.5 Data analysis

If not stated otherwise, all data analyses were performed using custom MATLAB (R2018b) code and built-in functions from the *Statistics and Machine Learning Toolbox*. In a few specific cases, R (v3.6.1) and RStudio (v1.2.1335) were used (see references to specific R packages below). The significance of all tests was evaluated at an alpha level of .05. Because the *F*-distribution is always asymmetric, reported *p*-values associated with repeated-measures analysis of variance (ANOVA) are directional (Winter, 2011). Partial Eta Squared (η_p^2) is provided as a standardized measures of effect size for ANOVAs.

2.5.1 Behavioral

The behavioral parameters that were analyzed were response times (RT) and accuracy (i.e., percentage of correct responses). Only target-present trials were considered. For accuracy measures, this selection of trials was required because in target-absent trials a correct target-absent-categorization (i.e., a volitional omission of a key press) could not be reliably dissociated from an incorrect, missing response. Mean RTs and accuracy measures per subject and condition were submitted to a repeated-measures ANOVA. Spatial demand and perceptual load served as within-subject factors.

2.5.2 EEG

All EEG data processing was performed using the open-source toolbox EEGLAB (v14.1.2; Delorme & Makeig, 2004) in combination with custom MATLAB (R2018b) code.

Preprocessing. The continuous EEG data were band-pass filtered, using a high-pass and a low-pass Hamming windowed sinc FIR filter. The lower edge of the frequency pass band was set to 0.1 Hz (filter order: 33000, transition band-width: 0.1 Hz, -6dB cutoff: 0.05 Hz) and the higher edge of the frequency pass band to 30 Hz (filter order: 440, transition band-width: 7.5 Hz, -6dB cut-off: 33.75 Hz). Then, channels with a normalized kurtosis (20% trimming before normalization) exceeding 5 standard deviations of the mean were rejected, using the automated channel rejection procedure implemented in EEGLAB. Malfunctioning channels that had to be switched off during the recording were identified using custom code and rejected as well. Altogether, one to nine channels were removed per participant ($M = 4.7$ channels). The data were re-referenced to the average of all remaining good-quality scalp channels, excluding EOG electrodes. Data epochs were extracted, ranging from -1000 to 4500 ms relative to target cue onset. For artifact rejection, an independent component analysis (ICA) was run on the dimensionality reduced data (using a basic PCA implementation). To speed up ICA decomposition, the data were down-sampled to 200 Hz prior to running the ICA algorithm. In addition, major artefacts and extremely large potential fluctuations were removed before running ICA, using the automatic trial-rejection procedure implemented in EEGLAB (i.e., function *pop_autorej*). The latter rejects data epochs, containing data values exceeding a given standard deviation threshold by means of an iterative procedure (probability threshold: 5 SD, maximum proportion of total trials rejection per iteration: 5%, threshold limit: 500 μ V). The obtained ICA decomposition was back-projected onto the original, continuous dataset (filtered and re-referenced) with a 1 kHz sampling rate. The latter was segmented into epochs ranging from -1000 to 4500 ms relative to target cue onset and baseline-corrected, using the pre-stimulus period of -200 to 0. To identify artefactual independent components (ICs), the EEGLAB plug-in ICLabel (v1.1, Pion-Tonachini, Kreutz-Delgado, & Makeig, 2019), was applied. ICLabel assigns a label vector to each IC, indicating the probability that an IC belongs to any of seven possible categories: brain, muscle, eye, heart, line noise, channel noise, or other. All ICs that received a probability estimate below 50% for the brain category were considered “artefactual” and

subsequently subtracted from the data. On average 34.12 ICs (i.e., 59.67 %) were removed per participants (SD = 3.53). Finally, the automatic trial rejection procedure implemented in EEGLAB was performed, setting the probability threshold to 5 SD, the maximum proportion of total trials to-be-rejected per iteration to 5 % and the threshold limit to 1000 μ V. On average, 269 trials (i.e., 22 %) were rejected in the course of this procedure (range 11 – 32 %). Lastly, data from channels that were initially rejected were interpolated using spherical interpolation. Note that this preprocessing pipeline only served as the basis for the univariate analysis of alpha-band power. For the multivariate decoding analysis, a simplified preprocessing pipeline was applied (cf. method section “*decoding analysis*”).

Time-frequency decomposition. The time-frequency decomposition of the processed EEG data was computed using Morlet wavelet convolution as implemented in the build-in EEGLAB STUDY functions (i.e., *newtimef.m*). Specifically, the segmented EEG signal was convolved with a series of complex Morlet wavelets. The frequencies of the wavelets ranged from 4 Hz to 30 Hz, increasing logarithmically in 52 steps. A complex Morlet wavelet is defined as a complex sine wave that is tapered by a Gaussian. The number of cycles, that defines the width of the tapering Gaussian, increased linearly as a function of frequency by a factor of 0.5. This procedure accounts for the trade-off between temporal and frequency precisions as a function of the frequency of the wavelet. The number of cycles at the lowest frequency was 3; the number of cycles at the highest frequency was 11.25. The time period in-between -400 and -100 ms relative to target cue onset served as a spectral baseline.

Alpha power lateralization. Spatial shifts of attention following the onset of the sound array were quantified by assessing lateralized modulations of posterior alpha-band power (8-12 Hz). Specifically, the difference between contralateral and ipsilateral alpha power at a cluster of posterior electrodes, comprising PO7/8, P7/8, P3/4, and PO3/4, was calculated separately for each condition and each subject. The selection of electrodes was based on previous studies of post-stimulus, posterior alpha lateralization (Klatt, Getzmann, Begau, & Schneider, 2019; Schneider, Göddertz, Haase, Hickey, & Wascher, 2019), except that P5/P6 were not part of the present electrode setup and thus, electrodes P3/4 were included in the electrode cluster instead. Given that post-stimulus alpha power asymmetries have been shown to appear as a relatively long-lasting, sustained effect, the mean contralateral-minus-ipsilateral

differences in power were extracted in a broad 400 ms-time window, ranging from 547 to 953 ms following sound array onset. The time window was set around the peak in the grand average contralateral minus ipsilateral difference waveform across all conditions and subjects. The peak was defined as the point in time at which the difference waveform (following sound array onset, 1600 ms – 3000 ms) reached its most negative amplitude value. The mean power values per subject and condition were then submitted to a repeated-measures ANOVA, including the within-subject factors *spatial demand* and *perceptual load* in order to assess their effect on alpha lateralization magnitude. For an analogous analysis of non-lateralized posterior alpha power, please see the supplementary material.

Alpha lateralization onset latencies. To quantify alpha lateralization onset latency, we used a combination of the fractional area technique (Kiesel, Miller, Jolicœur, & Brisson, 2008; Luck, 2014) and a jackknife approach (Luck, 2014; Miller, Patterson, & Ulrich, 1998). That is, for each condition, n subaverage contralateral minus ipsilateral difference waveforms were created, using a subsample of $n-1$ waveforms (i.e., each participant was omitted once). In each of these subaverage waveforms, the point in time at which the negative area under the curve reached 20% and 50%, respectively (i.e., Fractional Area Latency, denoted as FAL) was measured, using the MATLAB function *latency.m* by Liesefeld (2018). Negative area was measured relative to zero and in-between a broad time window from 1600 to 3000 ms post-cue-onset (i.e., 1600 ms corresponds to sound array onset). Note that reported mean latency differences (denoted as D) correspond to the differences in onset latency between conditions, measured in the condition-grand averages. According to Miller, Patterson, & Ulrich (1998), the jackknife-based SE_D was calculated as follows:

$$SE_D = \sqrt{\frac{N-1}{N} \sum_{i=1}^N (D_{-i} - \bar{J})^2}.$$

D_{-i} (for $i = 1, \dots, N$, with N representing the sample size) denotes the latency difference for the subsample, including all subject except for subject i . \bar{J} is the mean difference across all subsamples (i.e., $\bar{J} = \sum D_{-i} / N$).

The 20%-FAL and 50%-FAL values were submitted to separate repeated-measures ANOVAs, including the within-subject factors *spatial demand* and *perceptual load*. Because

the use of subsample average measures artificially reduces the error variance, the error terms in the respective ANOVA will be underestimated, while the F -values will be overestimated. To account for this bias, the F -correction according to Kiesel, Miller, Jolicœur, & Brisson (2008) was applied. Corrected F -values are denoted as F_{corr} . The corresponding p -value for the corrected F statistic was computed using the online calculator by Soper (2020).

Brain-behavior correlations. To investigate to what extent the timing of alpha lateralization was related to behavioral performance, we used a repeated-measures correlation approach and the R package *rmcorr* (Bakdash & Marusich, 2017). *Rmcorr* determines “the relationship between [...] two continuous variables, while controlling for the [...] between-participants variance” (Bakdash & Marusich, 2017, p. 3). We obtained FAL-measures from the single-subject waveforms (i.e., contralateral minus ipsilateral alpha power) for each of the four conditions and correlated those with condition-specific mean response times. Here, the latter were estimated, including only the (correct) trials that remained after EEG-artefact rejection. Three subjects did not show an alpha lateralization effect (i.e., there was no negative area) and were thus, excluded from the correlation analysis. The repeated-measures correlation coefficient r_{rm} as well as a 95% confidence interval will be reported. The corresponding degrees of freedom are calculated as follows (Bakdash & Marusich, 2017):

$$df_{rmcorr} = N(k - 1) - 1,$$

where k is the number of repeated measures per participant (i.e., 4) and N is the total number of participants (i.e., 14).

Decoding analysis. We attempted to decode the exact location (i.e., outer-left, inner-left, inner-right, outer-right) of the target sound based on the scalp distribution of alpha-band EEG power. The decoding procedure was applied separately for the *low* vs. the *high spatial demand* condition to investigate whether the ‘amount’ of spatial information reflected in the scalp topography of alpha-band power is modulated by the spatial demands of the task. The factor *perceptual load* was not considered in the decoding analysis. The decoding analysis described below was adapted from the analysis code and method provided by Bae & Luck

(2018). Note that for the present decoding analysis, no artifact rejection was performed on the EEG data. That is, the EEG preprocessing was limited to epoching the continuous data to create single-trial segments (i.e., ranging from -1000 to 4500 ms relative to cue onset) and baseline correction (i.e., using the 200 ms time period prior to cue onset as a baseline). Further, target-absent trials, incorrectly answered trials as well as trials with a response time < 200 (i.e., premature responses) were excluded. Running decoding analyses on neural time series data without artifact rejection and minimal preprocessing has previously been demonstrated to result in above-chance decoding accuracy (Grootswagers, Wardle, & Carlson, 2017) and prevents unwanted artefacts and spurious decoding due to high-pass (van Driel, Olivers, & Fahrenfort, 2021) or low-pass (Grootswagers et al., 2017) filtering. Instead, to improve the signal-to-noise ratio, after extracting alpha power from the signal, the data belonging to a given target location category were averaged across multiple trials. These averages (rather than single-trial data) served as the input for the to-be-trained classifier. The classifier was trained to discriminate between each target location and all other possible locations. To compute decoding accuracy, the classifier was then applied to the average of a set of trials for each location that was not part of the training data. Decoding was considered correct if the classifier correctly determined which one of the four possible locations was the target location. Thus, chance level decoding accuracy was at 25%.

Specifically, analogous to Bae & Luck (2018), the following decoding procedure was applied: The segmented EEG at all scalp electrodes was bandpass filtered at 8 to 12 Hz, using EEGLAB's *eegfilt()* function, which applies two-way least-squares finite impulse response (FIR) filtering. Then, the Hilbert transform of the bandpass filtered EEG signal was computed to obtain the magnitude of complex analytic signal. The latter was squared to obtain the total power in the alpha frequency band (i.e., 8-12 Hz) at each time point. Subsequently, to increase the efficiency of the analysis and decrease computation time, the data was subsampled, keeping only every 20th data point in-between -500 and 4500 ms relative to target sound onset (i.e., corresponding to a sampling rate of 50 Hz). This results in a 4-dimensional data matrix for each participant, including the dimensions of time (250 time points), location (4 different categories), trial (varies depending on the subject, in-between 68 and 112 trials for each location), and electrode site (the 57 scalp channels). To classify the location of the target sound based on the scalp topography of the alpha power signal over the 57 scalp electrodes (i.e., mastoids and EOG electrodes were excluded), we used a

combination of a support vector machine (SVM) and error-correcting output codes (ECOC; Dietterich & Balkiri, 1995). The ECOC model, implemented using the MATLAB function *fitcecoc()*, combines the results from multiple binary classifiers and thus, solves multiclass categorization problems.

Decoding was performed separately for each of the 250 time points in-between -500 and 4500 ms relative to target sound onset. At each time point, separate trials were used to train and test classifier performance, respectively. Specifically, a fivefold cross validation procedure was applied: First the data were sorted into four 'location bins', containing only trials with the same target location. In each location bin, the trials were divided into five equally sized sets of trials, each of which contained in-between 13 and 22 trials (depending on condition and subject, $MDN_{[lsd]} = 20$, $MDN_{[hsd]} = 18$). That is, to ensure that an equal number of trials was assigned to each of the five sets for each location bin, the minimum number of trials per subject for a given location bin was determined (denotes as n), and $n / 5$ trials were assigned to each set. In case the total trial number for a given location was not evenly divisible by five, excess trials were randomly omitted. The trials for a given location bin were averaged, resulting in a matrix of 5 (subsample averages) x 4 (location bins) x 57 (electrodes) to be analyzed for each time point. Notably, 4 of the 5 subsample averages served as the training set, while the remaining group average served as a testing dataset. In the training phase, the data from the four (of the total 5) subsample averages was simultaneously submitted to the ECOC model with known location labels to train four SVMs (one for each location). A one-versus-all approach was chosen such that each SVM was trained to perform a binary classification, that is, to discriminate one specific location from all other locations. Subsequently, in the test phase the unused data (i.e., the subsample average that were reserved for testing) was fed into the set of four trained SVMs to classify which of the 4 locations served as the target location in each of the subsample averages. Specifically, the MATLAB *predict()* function was used to classify the input data by minimizing the average binary loss across the four trained SVMs. Essentially, the output of the *predict()* function provides a location label for each of the 4 input subsample averages. By comparing the true location labels to the predicted location labels, decoding accuracy was computed.

This training-and-testing process was applied five times such that each subsample average served as the testing dataset once. Further, the entire procedure was iterated 10 times. On each iteration, the trials in each location bin were randomly assigned to the five

sets (i.e., to create new subsample averages). Finally, decoding accuracy was collapsed across the four locations, the five cycles of partitioning trials into sets, and the 10 iterations, resulting in a decoding percentage for each time point. After obtaining a decoding percentage for all time points of interest, a five-point moving average was applied to smooth the averaged decoding accuracy values and to minimize noise.

Statistical analysis of decoding accuracy. Although decoding was performed for all time points in-between -500 to 4500 ms relative to sound onset, the statistical analysis focused on the time interval following sound array presentation until the end of the maximal response interval (i.e., 1600 – 3800 ms relative to sound onset). We restricted the statistical analysis to this time interval because the goal was to test decoding accuracy during the post-stimulus interval (i.e., when post-stimulus attentional processing takes place). In addition, because participants did not have any knowledge about *where* the target is going to appear prior to sound array onset, there should be no location-specific information present in-between target cue and sound array-onset. Briefly, the statistical analysis of decoding accuracy comprised two separate approaches: First, to confirm that the scalp topography of post-stimulus alpha-band power contains information about the target location, we compared decoding accuracy to chance level (i.e., 25% – because we used 4 locations) at each time point. This was done separately for the two spatial demand conditions. Second, we compared decoding accuracy in the low and high spatial demand condition to evaluate whether the amount of spatial information that is reflected in the scalp topography of alpha-band power is sensitive to the spatial demands of the task. At both stages, we controlled for multiple comparisons (see below for details).

Decoding accuracy within conditions. We used a non-parametric cluster-based permutation analysis to compare decoding accuracy to chance level (i.e., 25%) at each time point. Again, we adopted the analysis code provided by Bae & Luck (2018). Using one-sided one sample *t*-tests, the average decoding accuracy across subjects was compared to chance level, separately for each time-point. Because SVM decoding does not produce meaningful below-chance decoding results, a one-sided *t*-test is justified. Then, clusters of at least two adjacent time points with a significant single-point *t*-test (i.e. $p < .05$) were identified. The *t*-values within a given cluster were summed, constituting the so-called cluster mass. To determine

whether a given cluster mass is greater than what can be expected under the null hypothesis, a Monte Carlo null distribution of cluster mass values was constructed. In a first step, this involved estimating the decoding accuracy that would be obtained if the classifier randomly guessed the target sound location. That is, from an array containing all possible target labels (1, 2, 3, 4), we randomly sampled an integer as the simulated response of the classifier for a given target location. If the response matched the true target value, the response was considered correct. This sampling procedure was repeated 200 times (4 locations x 5 cross-validations x 10 iterations) and for each time point of interest in-between 1600 ms to 3800 ms. The 200 scores for each time point were averaged to obtain the mean simulated decoding accuracy, resulting in a time series of decoding accuracy values. Analogous to the procedure that was applied to the actual EEG data, the latter was smoothed using a five-point running average filter. The procedure was repeated 17 times, to obtain a simulated decoding accuracy time series for each of our 17 participants. Then, using the simulated decoding accuracy time series, the maximum cluster mass was computed, using the procedure described above. That is, if there was more than one cluster of significant t -values, the mass of the largest cluster was selected.

Finally, to construct a null distribution of maximum cluster mass values that can be expected under the null hypothesis, we repeated the simulation procedure (i.e., simulating decoding accuracy that would be obtained by chance) 10,000 times. For each cluster in the decoding results, the obtained cluster t mass was compared to the distribution of cluster t mass values that was constructed under the assumption that the null hypothesis is true. If the observed cluster t mass value was in the top 95% of the null distribution (i.e. $\alpha = .05$, one-tailed), the null hypothesis was rejected and decoding accuracy was considered above chance. Note that this procedure was separately applied to both the low spatial demand condition and the high spatial demand condition.

To find the p -value associated with a specific cluster, we examined where within the null distribution does each observed cluster t mass value fall. That is, the p -value was based on the inverse percentile (computed using the *invprctile()* function) of the observed cluster-level t mass within the null distribution. If the observed cluster-level t -mass value exceeded the maximum cluster-level t -mass of the simulated null distribution, the respective p -value is reported as $p < 10^{-4}$. The latter corresponds to the resolution of the null distribution (i.e., 1 / number of permutations).

Decoding Accuracy in low vs. high spatial demand blocks. To investigate, whether or not the amount of spatial information reflected by the scalp topography of alpha power differs depending on the spatial demands of the task, decoding accuracy in the two task conditions was compared, using a cluster-corrected sign-permutation test. To this end, the *cluster_test()* and *cluster_test_helper()* functions provided by Wolff, Jochim, Akyürek, & Stokes (2017) were applied. The sign-permutation test is a non-parametric test that makes no assumption of the distribution of the data. As input data, the same time window that was also used for the statistical analysis of decoding accuracy within conditions was selected (i.e., 1600 – 3800 ms). Specifically, the *cluster_test_helper()* function generates a null distribution by randomly flipping the sign of the input data of each participant with a probability of 50%. This procedure was repeated 10,000 times. The resulting distribution served as input to the *cluster_test()* function, identifying those clusters in the actual data that are greater than would we expected under the null hypothesis. The cluster-forming threshold as well as the cluster significance threshold were set to $p < .05$. Because we had a clear hypothesis regarding the direction of the effect (that is, decoding accuracy in the high spatial demand condition should be higher compared to the low spatial demand condition), the cluster-corrected sign-permutation test was one-sided.

In addition, to assess the overall difference in decoding ability within the post-stimulus period, the decoding accuracy was averaged across time in the approximate time window that resulted in significant within-condition decoding results (i.e., 1800 – 3200 ms) and submitted to a one-sided permutation test. To this end, the *GroupPermTest()* function provided by Wolff et al. (2017) was applied (using $nSims = 10,000$ permutations).

2.6 Data/code availability statement

Data and analysis code associated with this manuscript will be made available in the open science framework repository upon publication of this manuscript.

3. Results

3.1 Behavioral data

Behavioral results are displayed in Figure 2. The analysis of response times revealed a main effect spatial demand, $F(1,16) = 68.75$, $p < .001$, $\eta_p^2 = 0.81$, with slower responses in high spatial demand blocks ($M = 834.79$ ms, $SD = 92.89$) compared to low spatial demand blocks

519 (M = 713.61 ms, SD = 123.94). In addition, there was a significant main effect of perceptual
 520 load, $F(1,16) = 161.57$, $p < .001$, $\eta_p^2 = 0.91$, with slower responses in high-load trials (M =
 521 843.92 ms, SD = 116.19) compared to low-load trials (M = 704.48 ms, SD = 98.47). For
 522 response times, there was no significant interaction of spatial demand and perceptual load,
 523 $F(1,16) = 2.59$, $p = .13$, $\eta_p^2 = 0.14$. A nearly analogous pattern of results was revealed by the
 524 analysis of the percentage of correct responses. That is, participants responded more
 525 accurately in low spatial demand blocks (M = 92.54 %, SD = 4.63) compared to high spatial
 526 demand blocks (M = 88.84 %, SD = 4.80), $F(1,16) = 21.58$, $p < .001$, $\eta_p^2 = 0.57$. In addition,
 527 the percentage of correct responses was higher in low-load trials (M = 96.57 %, SD = 2.72),
 528 compared to high-load trials (M = 84.81 %, SD = 7.32), $F(1,16) = 53.70$, $p < .001$, $\eta_p^2 = 0.77$.
 529 Further, a significant interaction of spatial demand and perceptual load, $F(1,16) = 10.78$, $p =$
 530 .005, $\eta_p^2 = .40$, complements the descriptive observation that the difference in accuracy
 531 between low and high perceptual load was slightly greater in high spatial demand blocks (M
 532 = 13.66 %, SD = 7.24) than in low spatial demand blocks (M = 9.87 %, SD = 6.82).

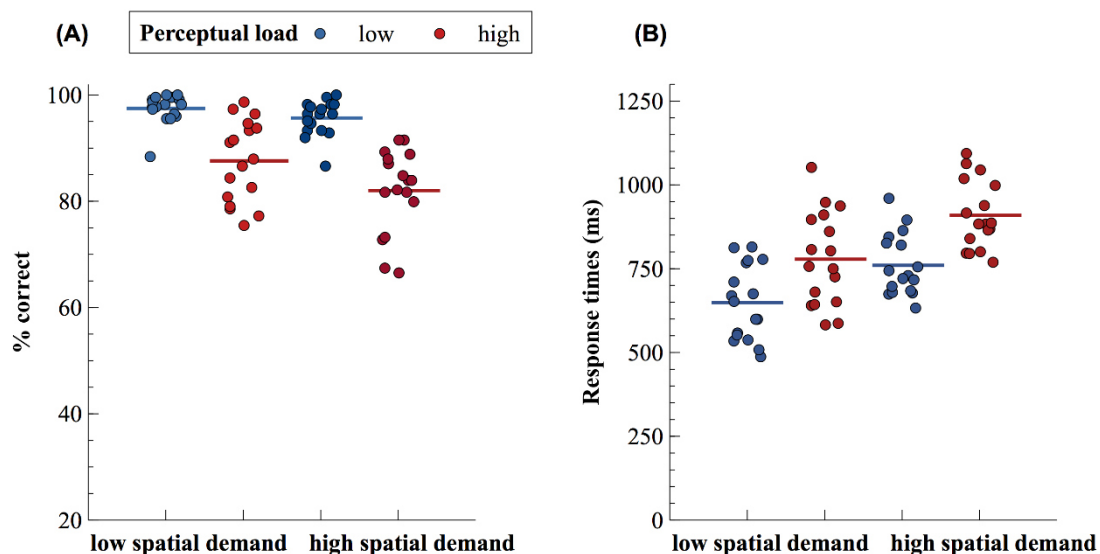


Figure 2. Behavioral performance. Solid, horizontal lines indicate the mean percentage of correct responses (A) or mean response times (B) in a given condition. Colored dots correspond to individual response measures. Please note that the y-axis for the % of correct responses does not originate at 0.

533 3.1 Alpha power lateralization

534 Figure 3A illustrates the time course of the contralateral minus ipsilateral differences in
 535 alpha power at a cluster of posterior scalp electrodes. A repeated-measures analysis of the

mean alpha power amplitudes in-between 547 to 953 ms post-sound array onset revealed no significant modulation by spatial demand, $F(1,16) < .001$, $p = .998$, $\eta_p^2 < 0.001$, neither by perceptual load, $F(1,16) = 0.04$, $p = .850$, $\eta_p^2 = 0.002$, nor an interaction between the two factors, $F(1,16) = 0.14$, $p = 0.710$, $\eta_p^2 = 0.009$.

540

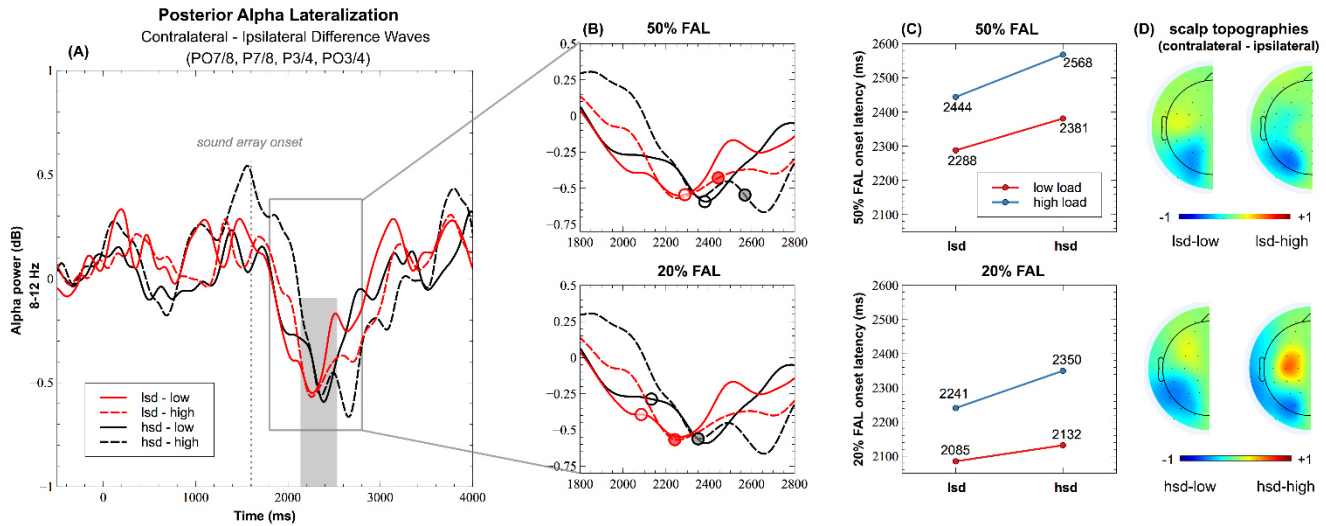


Figure 3. Alpha Power Lateralization. (A) Time course of contralateral minus ipsilateral differences in alpha power across a cluster of parieto-occipital scalp electrodes. The grey-filled rectangle highlights the time window used for statistical analysis of mean alpha lateralization magnitude. (B) A close-up view of the contralateral minus ipsilateral difference waveforms in-between 1800 and 2800 ms. Circles mark the 50% (top) and 20% (bottom) fractional area latency (FAL) measures for each condition. (C) A line plot of the respective 50%-FAL (top) and 20%-FAL (bottom) values, depending on spatial demand and perceptual load. (D) Scalp topographies based on the contralateral minus ipsilateral differences in alpha power in-between 547 to 953 ms following sound array onset (i.e., the time window used for statistical analyses).

541 3.2 Alpha lateralization onset latencies

542 To investigate whether the time-course of alpha lateralization was affected by the task
 543 demands, we assessed alpha lateralization onset latencies. Figure 3B and C illustrate the
 544 points in time where the area under the condition-specific difference curves reaches 20%
 545 and 50%, respectively (i.e., the 20% FAL and the 50% FAL). The analysis of fractional area
 546 latency (FAL) measures revealed a significant main effect of perceptual load for the 20%-FAL,
 547 $F_{\text{corr}}(1,16) = 5.94$, $p = .027$, and the 50%-FAL, $F_{\text{corr}}(1,16) = 9.17$, $p = .008$. That is, alpha
 548 lateralization emerged earlier in low perceptual load compared to high perceptual load trials
 549 ($D_{20\%} = 203$ ms, $SE_{D-20\%} = 68$, $D_{50\%} = 188$ ms, $SE_{D-50\%} = 52$). A significant main effect of spatial
 550 demand was only evident for the 50%-FAL, $F_{\text{corr}}(1,16) = 6.00$, $p = 0.026$, indicating earlier
 551 alpha lateralization onset latencies in low spatial demand blocks compared to high spatial

demand blocks ($D_{50\%} = 124$ ms, $SE_{D-50\%} = 57$). There were no significant interactions (all $F_{corr} < 0.73$).

3.2 Brain-behavior correlation

To assess, whether alpha lateralization onset latency varies with the behavioral response, we computed the repeated-measures correlation coefficient for the individual subject latency measures (i.e., no jackknifing was applied) and the individual mean response times. The latter approach considers the dependencies between the condition-specific measures and quantifies the common within-individual association across conditions. The analysis revealed a moderate positive relationship between onset latency and response times such that subjects with earlier alpha lateralization onset latencies showed shorter response times. This relationship was significant for both the 20%-FAL measures, $r_{rm}(41) = .365$, $p = .016$, 95% CI [0.065 0.605], and the 50%-FAL, $r_{rm}(41) = .373$, $p = .014$, 95% CI [0.073 0.610]. See Figure 4 for a scatter plot of the repeated-measures data, including all four conditions.

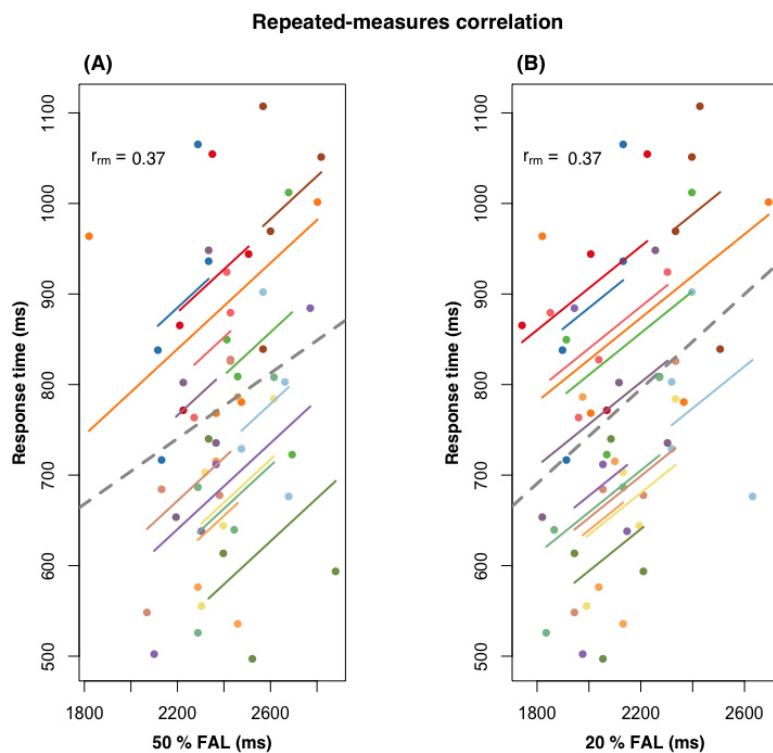


Figure 4. Repeated-measures correlation between alpha lateralization onset latency and response time. Each dot represents one of four separate observations for a participant, with observations from the same participants appearing in the same color. That is, each observation corresponds to a subject's mean response time (y-axis coordinate) and alpha lateralization onset latency (x-axis coordinate) in one of the four conditions. The corresponding colored lines show the rmcorr fit for each participant. Note that the rmcorr() function always fits parallel lines to the data (for details, see Bakdash & Marusich, 2017). The grey dashed line indicates the regression line that would result from treating the data as independent observations. Three subjects were excluded from the correlation analysis because they did not show an alpha lateralization effect (i.e., $n = 14$).

3.4 Decoding analysis

Figure 5A shows the time-course of decoding accuracy for the low vs. high spatial demand condition, when decoding the exact target sound location based on the topography of alpha-band activity, as well as the difference in decoding accuracy between conditions. Decoding accuracy starts to rise above chance level (i.e., 25%) at around 1800 ms (i.e., 200 ms following sound array onset) and at first, increases continuously in both spatial demand conditions. In the low spatial demand condition, decoding accuracy reaches a peak at around 2180 ms (i.e., 580 ms post-sound onset), remains at this level for a couple hundred milliseconds and then gradually decreases throughout the remainder of the response interval; in the high spatial demand condition, decoding accuracy continues to rise beyond the peak in the low spatial demand condition until around ~2440 ms (i.e., 840 ms post-sound onset), and declines quite immediately thereafter, although it remains on a higher level compared to the low spatial demand condition. Toward the end of the response interval (i.e., around 3800 ms), decoding accuracy returns to chance level in both conditions. The cluster mass test revealed that decoding was significantly greater than chance in both spatial demand conditions. We identified a significant cluster following sound array onset in each of the two conditions ($p < 10^{-4}$, see Figure 5A, solid green and yellow lines). In the high spatial demand condition, the cluster extends from around 1800 ms to ~3200 ms; in the low spatial demand condition, the cluster spans a time period in-between ~1900 ms and 2880 ms relative to sound array onset. Note, however, that cluster-based permutation test results should not be used to derive conclusions about the specific onset or offset of a certain effect (Sassenhagen & Draschkow, 2019).

The black, dashed line in Figure 5A illustrates the difference in decoding accuracy between the two spatial demand conditions. A cluster-corrected sign-permutation test indicated significant differences in decoding ability ($p < .01$, one-sided test, cluster extending from ~2440 – 3000 ms), with higher decoding accuracy in the high spatial demand condition compared to the low spatial demand condition.

Finally, we assessed the overall difference in decoding ability within the post-stimulus period (specifically, within the approximate time-window that resulted in above-chance decoding accuracy within both spatial demand conditions). A one-sided permutation test of the average decoding accuracy between 1800 – 3200 ms consistently revealed a significant difference in decoding accuracy between the spatial demand conditions ($p = .001$, Fig. 5B).

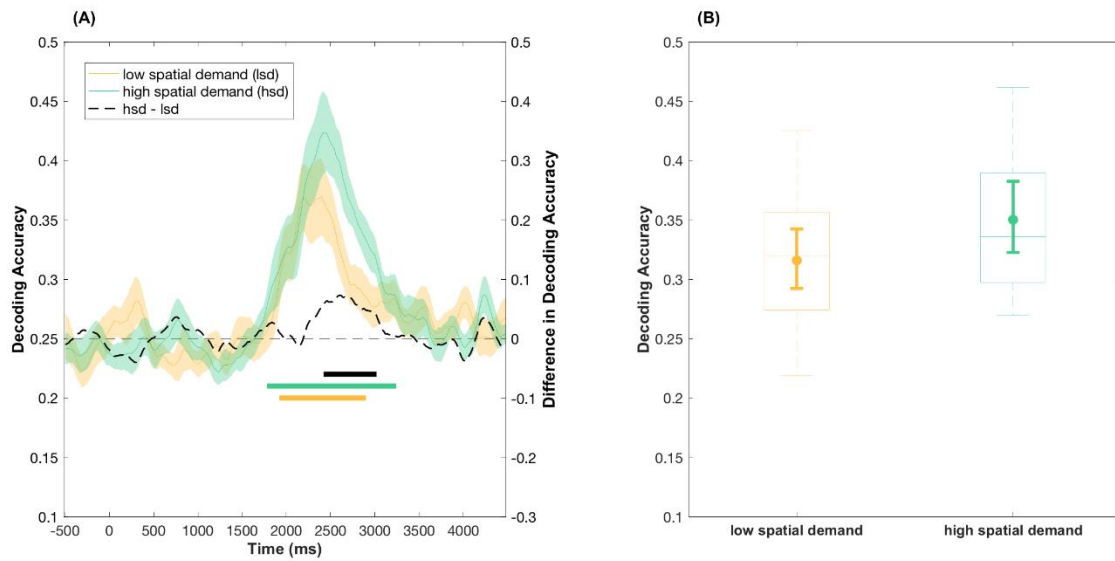


Figure 5. Location decoding based on the multivariate scalp distribution of alpha power. (A) Time-course of the average decoding accuracy results in the low (yellow) and high (green) spatial demand condition, respectively. The colored shading indicates ± 1 SEM. Chance-level performance (i.e., 25%) is indicated by the grey dashed horizontal line. The yellow and green solid bars indicate significant decoding of the target location in the low and high spatial demand condition, respectively. The black solid bar denotes significant differences in decoding ability between the low and the high spatial demand condition. Note that only time-points in-between 1600 – 3800 ms were considered in the statistical analysis. (B) Boxplots refer to the average decoding accuracy in-between 1800 – 3200 ms relative to cue-onset (i.e., 200 – 1600 ms following sound array onset). As per convention, boxplots illustrate the interquartile range and the median. Whiskers extent to the 1.5 times the interquartile range. The superimposed circles show the average decoding accuracy, while the corresponding error bars denote the 95% bootstrap confidence interval of the mean (number of bootstrap samples = 10000).

4. Discussion

Sensory stimuli and behavioral demands are constantly subject to change, requiring the attentive brain to adapt its response to accommodate to those changes. In this study, we investigated the effects of varying perceptual load and spatial demand in a sound localization task on post-stimulus alpha-band oscillations. The notion that alpha-band oscillations track the currently attended location in a spatially fine-tuned manner is relatively undisputed. However, what remains more elusive is to what degree this spatial specificity depends on the current task demands. Here, we demonstrate that the amount of spatial information reflected in the multivariate scalp distribution of alpha power increases when the task requires a precise sound localization (i.e., indicating the exact stimulus location) compared to when a rather coarse localization judgment is required (i.e., indicating the hemifield). In contrast, these task demand-dependent modulations were not captured by

the magnitude of univariate parieto-occipital alpha lateralization. Rather, the time course of alpha power lateralization varied with the task demands as well as with response times.

Behaviorally, the pattern of results was consistent with the well-established observation that the detection of a target sound in a cocktail-party scenario suffers from additional concurrent stimuli in the auditory scene (Brungart & Simpson, 2007; Brungart, Simpson, Ericson, & Scott, 2001; Ericson, Brungart, & Simpson, 2004; Klatt et al., 2018b). Accordingly, in the present study, participants performed slower and less accurate when the sound array contained four (high perceptual load) instead of just two sounds (low perceptual load). In terms of sound localization accuracy, this difference was even more pronounced when they were asked to report the exact target location (high spatial demand) rather than the target hemifield (low spatial demand). Certainly, the present set size effect cannot be completely disentangled from the effects of energetic masking due to the acoustic overlap between the competing sound sources (cf. Murphy, Spence, & Dalton, 2017). However, most critical for the intended EEG analysis was the manipulation of spatial demand. As expected, indicating the exact sound location was more challenging (i.e., slower and less accurate) than simply determining whether the target was present in the left or right hemispace. Nevertheless, subjects still managed to perform clearly above chance level (i.e., on average > 80% correct).

The main question of the present study was: Is the difference in spatial task demands also reflected in the neural signal? Strikingly, while the classifier could reliably decode the precise target location in both spatial demand conditions, the amount of spatial information reflected in the scalp distribution of alpha-band power was higher under high spatial demand. It should be emphasized that in both spatial demand conditions, participants were presented with the exact same trials (although in randomly shuffled order). This rules out that differences between conditions were caused by bottom-up perceptual factors.

The present results extend previous work, using an analogous auditory search task design, where we demonstrated that the presence of auditory post-stimulus alpha lateralization was dependent on the task-relevance of spatial information. Specifically, Klatt et al. (2018b) showed that alpha lateralization was absent in a simple sound detection task (i.e., when spatial location was completely irrelevant to the task), whereas it reliably indicated the attended location when participants were asked to localize the target. Here, we show that post-stimulus alpha oscillations are not only sensitive to such coarse manipulations of spatial relevance, but rather – when considering the multivariate activity

patterns – also capture fine-grained adaptations to the required degree of spatial specificity. However, the curves reflecting decoding accuracy in the low and high spatial demand conditions do not diverge until about 600 ms following sound array onset; in addition, statistically significant differences in decoding accuracy were limited to a relatively late time-window (i.e., > 800 ms following sound array onset; cf. Figure 5A). In contrast, general decodability of spatial location increases above chance level shortly after sound array onset and persists well into the response interval. This suggests that, despite the fact that the spatial demand conditions were blocked (i.e., participants knew beforehand which spatial specificity would be required), it took several hundred milliseconds to evoke changes in spatial specificity of the underlying alpha power signal. Such long latencies have also been reported with respect to voluntary adaptations of the alpha-power signal in a visual spatial cueing study paradigm, requiring participants to adopt either a narrow or a broad focus of attention in anticipation of an upcoming search array (Feldmann-Wüstefeld & Awh, 2019).

In the above-mentioned study, Feldmann-Wüstefeld & Awh (2019) computed spatially selective channel tuning functions (CTF) based on the topography distribution of alpha power and assessed their slope as a measure of spatial selectivity. Notably, differences in the CTF slopes between the narrow-focus cue and the broad-focus cue only emerged at timepoints > 500 ms following cue onset. A previous study by Voytek and colleagues (Voytek et al., 2017) similarly manipulated the breadth of the attentional focus using a central cue, pointing to either the exact location the target will appear in or to an approximate region of varying size. Consistent with Feldmann-Wüstefeld & Awh (2019), an inverted encoding modeling analysis revealed that the spatial selectivity of anticipatory alpha-band activity decreased with greater uncertainty about the upcoming target's location.

Critically, the present results add to these previous findings in several ways: First, we demonstrate that just like preparatory attention is finely tuned and spatially sharpened depending on the task demands (Feldmann-Wüstefeld & Awh, 2019; Voytek et al., 2017), the ongoing attentional processing following search array onset is dynamically modulated depending on the required spatial specificity of the task. Further, the present findings complement a growing body of evidence, supporting the assumption that modulations of alpha oscillations represent a ubiquitous top-down controlled mechanism of spatial attention that plays a role across different attentional domains as well as across sensory modalities.

In principle, the notion that attention can improve the information content of a neural code is not novel. In fact, it is well-established that attending to a spatial position or a relevant feature increases single-neuron firing rates in primary and extrastriate visual areas and can result in changes in the size and position of spatial receptive fields (reviewed by (Sprague, Saproo, Serences, Jolla, & Jolla, 2015). In the auditory domain, physiological recordings in cats (Lee & Middlebrooks, 2011) revealed similar sharpening of spatial tuning in auditory cortex (i.e., A1) when the animal engaged in a spatial task compared to an off-task “Idle” condition and a non-spatial periodicity detection task (for similar findings in human A1 see van der Heijden, Rauschecker, Formisano, Valente, & de Gelder, 2018). Hence, along with previous studies in the visual modality (Feldmann-Wüstefeld & Awh, 2019; Voytek et al., 2017), the present results extend these findings, showing that such “sharpening” of neural activity occurs not only in tuning functions of single neurons, but is also evident in the adaption of population-level activity patterns.

In addition to the multivariate decoding analysis, we also analyzed alpha lateralization following sound array onset as a ‘classical’ univariate measure of attentional orienting (e.g., Ikkai, Dandekar, & Curtis, 2016). In the present study, alpha lateralization magnitude did neither vary with perceptual load or spatial demand. The former observation replicates results of a previous study (Klatt et al., 2018b), finding no evidence for differences in alpha lateralization magnitude between a low-load (i.e., two-sound array) and a high-load (i.e., four-sound array) auditory search condition. In contrast, Bacigalupo and Luck (2019) reported that target-elicited alpha lateralization in a visual search paradigm tended to increase with greater task difficulty. Thus, the authors speculate that alpha lateralization might reflect effort rather than target selection. The present findings do not seem to bolster this claim: Both the behavioral data as well as a supplementary analysis of non-lateralized posterior alpha power (cf. supplementary material, S1) indicate that task difficulty and required cognitive resources increased with greater spatial demand. Yet, alpha lateralization magnitude was unaffected by the experimental manipulation. Nonetheless, the present findings do substantiate the notion that post-stimulus (or target-elicited) alpha lateralization presents an active signature of target processing in both visual (Bacigalupo & Luck, 2019) as well as auditory search (Klatt et al., 2018b). Bacigalupo and Luck (2019) further dissociate alpha lateralization from a well known ERP-signature of target individuation (i.e., the N2pc), suggesting that alpha lateralization reflects a long-lasting and ongoing attentional processing

of the target. Although we do not investigate ERP correlates in the present study, a closer look at the time-course of alpha lateralization supports this assumption: on average, alpha lateralization persist beyond and in fact peaks around the time participants make their response. Different temporal characteristics of N2ac (an auditory analogue of the visual N2pc component Gamble & Luck, 2011) and alpha lateralization have recently also been observed in response to shifts of auditory attention between relevant talkers in a simulated cocktailparty scenario (Getzmann, Klatt, Schneider, Begau, & Wascher, 2020), corroborating the notion that the EEG measures reflect different attentional processes (see also Klatt et al., 2018b).

Contrary to alpha lateralization magnitude, alpha lateralization onset latency was tightly linked to task difficulty and moreover, to behavioral performance. Specifically, alpha lateralization emerged up to 203 ms earlier (20%-FAL) in the less demanding low perceptual load condition relative to the high perceptual load condition and 123 ms earlier (50%-FAL) in the low spatial demand condition relative to the high spatial demand condition. Furthermore, a repeated-measures correlation analysis showed that across all conditions, participants with earlier alpha lateralization onset latency showed shorter response times. This association was of moderate size ($r_{rm} = .37$), irrespective of whether the 20%-FAL or 50%-FAL was considered. This illustrates that slower sound localization coincides with slower post-stimulus attentional processing, which is reflected in delayed alpha lateralization onset latencies. Overall, this is in line with a previous visual search study (Foster et al., 2017), showing that the onset of alpha-based CTFs varied with reaction times as well as search difficulty. That the latency differences reported by Foster et al. (2017) were much larger (i.e., differences of up to 440 ms) could be attributed to the fact that their search conditions differed more strongly (e.g., distractors were all identical vs. heterogenous). In sum, the present findings corroborate the claim that attentional modulations of alpha power not only track the location of covert spatial attention, but also the time-course (i.e., the latency) of post-stimulus attentional processing.

Finally, the clear-cut difference between univariate and multivariate measures of alpha power highlights the potential of multivariate decoding for the study of neurocognitive mechanisms. Similarly, when performing a univariate analysis of alpha power, Voytek et al. (2017) did not capture the fine-grained differences in the allocation of attention (depending on the spatial certainty of a cue) that were evident in the multivariate topography of alpha

power. Taken together, this illustrates the increased sensitivity of multivariate decoding techniques to reveal complex dynamics that are present in the combined signal across the scalp (Hebart & Baker, 2017).

5. Conclusion

In conclusion, our results show that the spatial specificity of post-stimulus alpha-band oscillations can be finely adapted depending on the spatial demands of the task. Notably, this task-dependent adaptation was only captured by the multivariate distribution of the alpha-band signal, whereas the magnitude of parieto-occipital alpha lateralization was insensitive to both variations in perceptual load and spatial demand. Yet, we observed a clear-cut association between alpha lateralization onset latency and response times in the present sound localization task. Thus, it appears that the time-resolved modulation of post-stimulus alpha lateralization clearly captures differences in the efficiency of post-attentional processing, which in turn affects behavioral outcomes. These findings improve our understanding of the functional role of alpha oscillations for the ongoing attentional processing of complex auditory scenes and provide new insights into the attentional mechanisms underlying top-down adaptations to changing task demands.

6. Competing Interests

Declarations of interest: none.

7. Author contributions: CRediT authors statement

Laura-Isabelle Klatt: Conceptualization, Formal analysis, Investigation, Writing – Original Draft, Visualization, Project administration **Stephan Getzmann:** Conceptualization, Writing- Review & Editing, Supervision **Daniel Schneider:** Conceptualization, Writing- Review & Editing, Supervision

8. Acknowledgements

The authors would like to thank Peter Dillmann for the technical implementation of the stimulus presentation software and Tobias Blanke for technical support. Further, the authors are grateful to the lab staff, in particular to Pia Deltenre and Barbara Foschi, and their team of student assistants for their help with data acquisition. In addition, many thanks go to Gi-

Yeul Bae and Steven Luck as well as Michael J. Wolff and colleagues for publicly sharing their code (Bae & Luck, 2018; Wolff et al., 2017), which served as the basis for the present decoding and cluster permutation analyses.

9. References

- Anton-Erxleben, K., & Carrasco, M. (2013, March). Attentional enhancement of spatial resolution: Linking behavioural and neurophysiological evidence. *Nature Reviews Neuroscience*, Vol. 14, pp. 188–200. <https://doi.org/10.1038/nrn3443>
- Bacigalupo, F., & Luck, S. J. (2019). Lateralized suppression of alpha-band EEG activity as a mechanism of target processing. *Journal of Neuroscience*, 39(5), 900–917. <https://doi.org/10.1523/JNEUROSCI.0183-18.2018>
- Bae, G.-Y., & Luck, S. J. (2018). Dissociable Decoding of Spatial Attention and Working Memory from EEG Oscillations and Sustained Potentials. *The Journal of Neuroscience*, 38(2), 409–422. <https://doi.org/10.1523/JNEUROSCI.2860-17.2017>
- Bahramisharif, A., Heskens, T., Jensen, O., & van Gerven, M. A. J. (2011). Lateralized responses during covert attention are modulated by target eccentricity. *Neuroscience Letters*, 491, 35–39. <https://doi.org/10.1016/j.neulet.2011.01.003>
- Bakdash, J. Z., & Marusich, L. R. (2017). Repeated measures correlation. *Frontiers in Psychology*, 8(MAR), 1–13. <https://doi.org/10.3389/fpsyg.2017.00456>
- Brungart, D. S., & Simpson, B. (2007). Cocktail party listening in a dynamic multitalker environment. *Perception & Psychophysics*, 69(1), 79–91.
- Brungart, D. S., Simpson, B. D., Ericson, M. A., & Scott, K. R. (2001). Informational and energetic masking effects in the perception of multiple simultaneous talkers. *The Journal of the Acoustical Society of America*, 110(5), 2527–2538. <https://doi.org/10.1121/1.1408946>
- Carrasco, M., & McElree, B. (2001). Covert attention accelerates the rate of visual information processing. *Proceedings of the National Academy of Sciences of the United States of America*, 98(9), 5363–5367. <https://doi.org/10.1073/pnas.081074098>
- Carrasco, M., Penpeci-Talgar, C., & Eckstein, M. (2000). Spatial covert attention increases contrast sensitivity across the CSF: Support for signal enhancement. *Vision Research*, 40(10–12), 1203–1215. [https://doi.org/10.1016/S0042-6989\(00\)00024-9](https://doi.org/10.1016/S0042-6989(00)00024-9)
- Delorme, A., & Makeig, S. (2004). EEGLAB: an open source toolbox for analysis of single-trial

EEG dynamics including independent component analysis. *Journal of Neuroscience Methods*, 134(2004), 9–21. <https://doi.org/10.1016/j.jneumeth.2003.10.009>

Deng, Y., Choi, I., & Shinn-Cunningham, B. G. (2020). Topographic specificity of alpha power during auditory spatial attention. *NeuroImage*, 207, 116360. <https://doi.org/10.1016/j.neuroimage.2019.116360>

Dietterich, T. G., & Balkiri, G. (1995). Solving Multiclass Learning Problems via Error-Correcting Output Codes. *Journal of Artificial Intelligence Research*, 2, 263–286.

Ericson, M. A., Brungart, D. S., & Simpson, B. D. (2004). Factors That Influence Intelligibility in Multitalker Speech Displays. In *The International Journal of Aviation Psychology* (Vol. 14). <https://doi.org/10.1207/s15327108ijap1403>

Feldmann-Wüstefeld, T., & Awh, E. (2019). Alpha-band activity tracks the zoom lens of attention. *Journal of Cognitive Neuroscience*, 32(2), 272–282. https://doi.org/10.1162/jocn_a_01484

Foster, J. J., Sutterer, D. W., Serences, J. T., Vogel, E. K., & Awh, E. (2017). Alpha-band oscillations enable spatially and temporally resolved tracking of covert spatial attention. *Psychological Science*, 28(7), 929–941. <https://doi.org/10.1177/0956797617699167>

Foxe, J. J., Simpson, G. V., & Ahlfors, S. P. (1998). Parieto-occipital ~10 Hz activity reflects anticipatory state of visual attention mechanisms. *NeuroReport*, 9(17), 3929–3933. <https://doi.org/10.1097/00001756-199812010-00030>

Gamble, M. L., & Luck, S. J. (2011). N2ac: An ERP component associated with the focusing of attention within an auditory scene. *Psychophysiology*, 48(8), 1057–1068. <https://doi.org/10.1111/j.1469-8986.2010.01172.x>

Getzmann, S., Klatt, L. I., Schneider, D., Begau, A., & Wascher, E. (2020). EEG correlates of spatial shifts of attention in a dynamic multi-talker speech perception scenario in younger and older adults. *Hearing Research*, 398, 108077. <https://doi.org/10.1016/j.heares.2020.108077>

Grootswagers, T., Wardle, S. G., & Carlson, T. A. (2017). Decoding dynamic brain patterns from evoked responses: A tutorial on multivariate pattern analysis applied to time series neuroimaging data. *Journal of Cognitive Neuroscience*, 29(4), 677–697. https://doi.org/10.1162/jocn_a_01068

Hebart, M. N., & Baker, C. I. (2017). Deconstructing multivariate decoding for the study of brain function. *NeuroImage*, (201 7).

834 <https://doi.org/10.1016/j.neuroimage.2017.08.005>

835 Ikka, A., Dandekar, S., & Curtis, C. E. (2016). Lateralization in alpha-band oscillations predicts
836 the locus and spatial distribution of attention. *PLoS One*, 11(5), e0154796.
837 <https://doi.org/10.1371/journal.pone.0154796>

838 Kiesel, A., Miller, J., Jolicœur, P., & Brisson, B. (2008). Measurement of ERP latency
839 differences: A comparison of single-participant and jackknife-based scoring methods.
840 *Psychophysiology*. <https://doi.org/10.1111/j.1469-8986.2007.00618.x>

841 Klatt, L.-I., Getzmann, S., Begau, A., & Schneider, D. (2019). A dual mechanism underlying
842 retroactive shifts of auditory spatial attention: dissociating target- and distractor-
843 related modulations of alpha lateralization. *Scientific Reports*, 10, 13860.
844 <https://doi.org/10.1101/2019.12.19.882324>

845 Klatt, L.-I., Getzmann, S., Wascher, E., & Schneider, D. (2018a). Searching for auditory targets
846 in external space and in working memory: Electrophysiological mechanisms underlying
847 perceptual and retroactive spatial attention. *Behavioural Brain Research*, 353, 98–107.
848 <https://doi.org/10.1016/j.bbr.2018.06.022>

849 Klatt, L.-I., Getzmann, S., Wascher, E., & Schneider, D. (2018b). The contribution of selective
850 spatial attention to sound detection and sound localization: Evidence from event-
851 related potentials and lateralized alpha oscillations. *Biological Psychology*, 138, 133–
852 145. <https://doi.org/10.1016/j.biopsycho.2018.08.019>

853 Lee, C.-C., & Middlebrooks, J. C. (2011). Auditory Cortex Spatial Sensitivity Sharpens During
854 Task Performance. *Nature Neuroscience*, 14(1), 108–114.
855 <https://doi.org/doi:10.1038/nn.2713>.

856 Liesefeld, H. R. (2018). Estimating the Timing of Cognitive Operations With MEG / EEG
857 Latency Measures : A Primer , a Brief Tutorial , and an Implementation of Various
858 Methods. *Frontiers in Neuroscience*, 12(October), 1–11.
859 <https://doi.org/10.3389/fnins.2018.00765>

860 Luck, S. J. (2014). *An introduction to the event-related potential technique* (2nd ed.). MIT
861 Press.

862 Miller, J., Patterson, T., & Ulrich, R. (1998). Jackknife-based method for measuring LRP onset
863 latency differences. *Psychophysiology*, 35(1), 99–115. [https://doi.org/10.1111/1469-](https://doi.org/10.1111/1469-8986.3510099)
864 [8986.3510099](https://doi.org/10.1111/1469-8986.3510099)

865 Murphy, S., Spence, C. J., & Dalton, P. (2017). Auditory perceptual load: A review. *Hearing*

866 *Research*, 352, 40–48. <https://doi.org/10.1016/j.heares.2017.02.005>

867 Oldfield, R. C. (1971). The assessment and analysis of handedness: the Edinburgh inventory.

868 *Neuropsychologia*, 9, 97–113. Retrieved from

869 <http://www.ncbi.nlm.nih.gov/pubmed/5146491>

870 Pion-Tonachini, L., Kreutz-Delgado, K., & Makeig, S. (2019). ICLabel: An automated

871 electroencephalographic independent component classifier, dataset, and website.

872 *NeuroImage*, 198, 181–197. <https://doi.org/10.1016/j.neuroimage.2019.05.026>

873 Poch, C., Capilla, A., Hinojosa, J. A., & Campo, P. (2017). Selection within working memory

874 based on a color retro-cue modulates alpha oscillations. *Neuropsychologia*, 106, 133–

875 137. <https://doi.org/10.1016/j.neuropsychologia.2017.09.027>

876 Popov, T., Gips, B., Kastner, S., & Jensen, O. (2019). Spatial specificity of alpha oscillations in

877 the human visual system. *Human Brain Mapping*, (June), 1–9.

878 <https://doi.org/10.1002/hbm.24712>

879 Rihs, T. A., Michel, C. M., & Thut, G. (2007). Mechanisms of selective inhibition in visual

880 spatial attention are indexed by α -band EEG synchronization. *European Journal of*

881 *Neuroscience*, 25(2), 603–610. <https://doi.org/10.1111/j.1460-9568.2007.05278.x>

882 Sassenhagen, J., & Draschkow, D. (2019). Cluster-based permutation tests of MEG/EEG data

883 do not establish significance of effect latency or location. *Psychophysiology*, 56(6),

884 e13335. <https://doi.org/10.1111/psyp.13335>

885 Schneider, D., Göddertz, A., Haase, H., Hickey, C., & Wascher, E. (2019). Hemispheric

886 asymmetries in EEG alpha oscillations indicate active inhibition during attentional

887 orienting within working. *Behavioural Brain Research*, 359, 38–46.

888 <https://doi.org/10.1016/j.bbr.2018.10.020>

889 Schneider, D., Mertes, C., & Wascher, E. (2016). The time course of visuo-spatial working

890 memory updating revealed by a retro-cuing paradigm. *Scientific Reports*, 6, 21442.

891 <https://doi.org/10.1038/srep21442>

892 Soper, D. S. (2020). p-Value Calculator for an F-Test [Software]. Retrieved December 16,

893 2020, from <https://www.danielsoper.com/statcalc>

894 Sprague, T. C., Saproo, S., Serences, J. T., Jolla, L., & Jolla, L. (2015). Visual attention mitigates

895 information loss in small- and large scale neural codes. *Trends in Cognitive Sciences*,

896 19(4), 215–226. <https://doi.org/10.1016/j.tics.2015.02.005>

897 van der Heijden, K., Rauschecker, J. P., Formisano, E., Valente, G., & de Gelder, B. (2018).

- Active sound localization sharpens spatial tuning in human primary auditory cortex. *Journal of Neuroscience*, 38(40), 8574–8587. <https://doi.org/10.1523/JNEUROSCI.0587-18.2018>
- van Driel, J., Olivers, C. N. ., & Fahrenfort, J. J. (2021). High-pass filtering artifacts in multivariate classification of neural time series data. *Journal of Neuroscience Methods*, 352, 109080. <https://doi.org/10.1101/530220>
- Voytek, B., Samaha, J., Rolle, C. E., Greenberg, Z., Gill, N., Porat, S., ... Gazzaley, A. (2017). Preparatory encoding of the fine scale of human spatial attention. *Journal of Cognitive Neuroscience*, 29(7), 1302–1310. https://doi.org/10.1162/jocn_a_01124
- Winter, B. (2011). The F distribution and the basic principle behind ANOVAs. Retrieved from http://menzerath.phonetik.uni-frankfurt.de/teaching/R/bw_anova_general_HR.pdf
- Wolff, M. J., Jochim, J., Akyürek, E. G., & Stokes, M. G. (2017). Dynamic hidden states underlying working-memory-guided behavior. *Nature Neuroscience*, 20(6), 864–871. <https://doi.org/10.1038/nn.4546>
- Worden, M. S., Foxe, J. J., Wang, N., & Simpson, G. V. (2000). Anticipatory biasing of visuospatial attention indexed by retinotopically specific α -band electroencephalography increases over occipital cortex. *The Journal of Neuroscience*, 20(6), RC63. <https://doi.org/10.1523/JNEUROSCI.20-06-j0002.2000>

SUPPLEMENTARY MATERIALS FOR

Attentional Modulations of Alpha Power Are Sensitive to the Task-relevance of Auditory Spatial Information

Laura-Isabelle Klatt, Stephan Getzmann, Daniel Schneider

Leibniz Research Centre for Working Environment and Human Factors

S1. Non-lateralized, posterior alpha power desynchronization as a measure of cognitive task demands

Desynchronization of alpha-band activity, resulting in low levels of alpha power, has been linked with states of high excitability and thus, thought to reflect functional engagement and information processing. Accordingly, increased working memory load (Fukuda, Mance, & Vogel, 2015; Krause et al., 2000) or greater semantic elaboration in an encoding task (Hanslmayr, Spitzer, & Bäuml, 2009) have been shown to coincide with greater event-related desynchronization (ERD). In the present study, posterior alpha ERD served as a measure of cognitive task demands. Mean alpha ERD amplitude per condition and subject was measured in-between 2160 and 2260 ms relative to target cue onset (i.e., 560 – 660 ms relative to sound array onset) at electrode Pz. Figure S1 depicts the condition-specific average waveforms of posterior alpha power. The time window that served as the basis for the statistical analysis was determined using a collapsed localizer approach (Luck & Gaspelin, 2017). That is, we assessed the negative peak in the grand average waveform across conditions in a broad time-window from 1600 ms to 3000 ms (relative to target cue onset; i.e., the same time window used to measure the area under the curve for fractional area latency measurement). A 100 ms time window (i.e., +/- 50 ms) around the resulting peak value of 2210 ms constituted the measurement time window. Mean alpha power values were then submitted to a repeated-measures ANOVA, including the within-subject factors *spatial demand* (high vs. low) and *perceptual load* (high vs. low). The analysis revealed a significant main effect of spatial demand, $F(1,16) = 7.87$, $p = .013$, $\eta_p^2 = 0.34$, reflecting greater alpha ERD (i.e., more negative power) in the high spatial demand condition ($M = -3.78$ dB, $SD = 2.43$) compared to the low spatial demand condition ($M = -3.06$ dB, $SD = 2.10$). While the main effect perceptual load was not significant, $F(1,16) = 0.44$, $p = .52$, $\eta_p^2 = .03$, there was a significant interaction between spatial demand and perceptual load, $F(1,16) =$

24 10.01, $p = .006$, $\eta_p^2 = 0.38$. Follow-up paired sample t -tests revealed that the difference
 25 between low and high perceptual load trials fell short of significance in both the low spatial
 26 demand condition, $t(16) = 1.78$, $p = .094$, $p_{adj} = .233$, $g = 0.20$, and the high spatial demand
 27 condition, $t(16) = -1.49$, $p = .155$, $p_{adj} = .233$, $g = -0.08$. Note that fdr -corrected (Benjamini &
 28 Yekutieli, 2001) p -values are denoted as p_{adj} , whereas g refers to Hedges' g (Hentschke &
 29 Stüttgen, 2011). Altogether, the results complement the behavioral data analysis in the main
 30 manuscript, confirming that in particular the high spatial demand condition required a
 31 higher amount of cognitive resources compared to the less demanding low spatial demand
 32 condition.

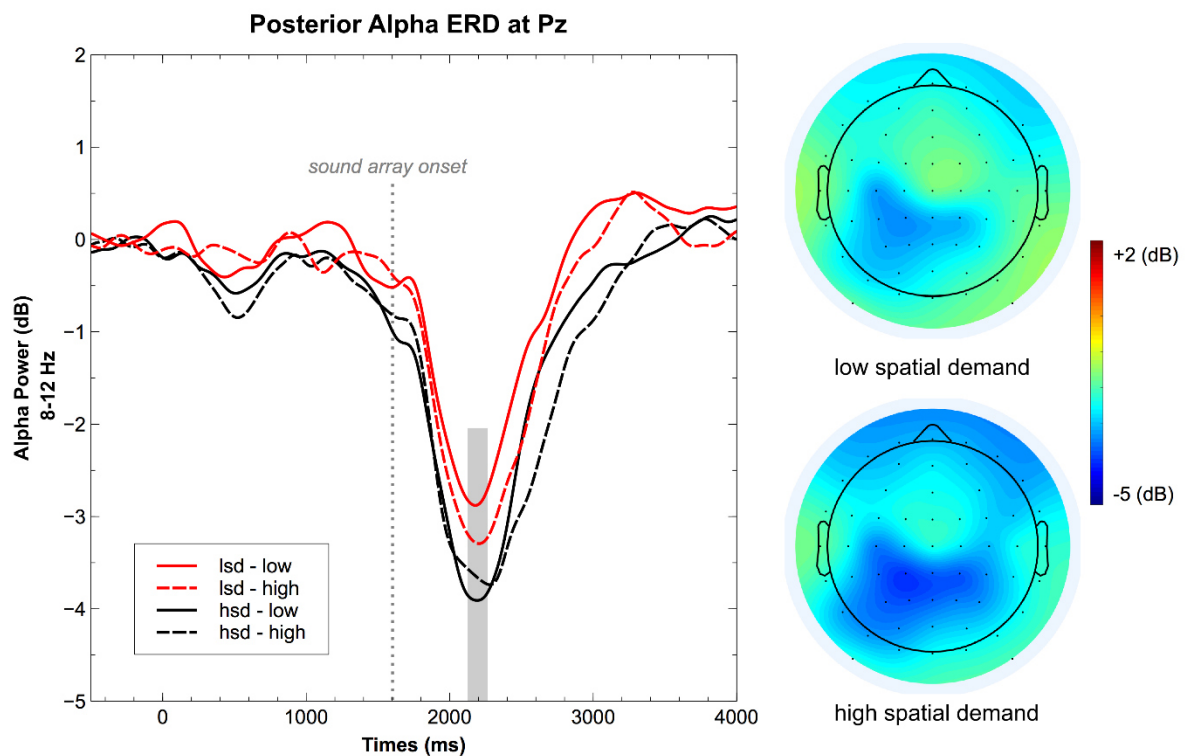


Figure S1. Event-related desynchronization (ERD) of alpha power at Pz. The line plot illustrates the condition-specific averages depending on spatial demand and perceptual load. lsd-low = low spatial demand / low perceptual load, lsd-high = low spatial demand / high perceptual load, hsd-low = high spatial demand / low perceptual load, hsd-high = high spatial demand / high perceptual load. The grey rectangle indicates the approximate time window used for statistical analysis (i.e., 2160 and 2260 ms relative to target cue onset). Accordingly, the scalp topographies are based on the average alpha power in the respective analysis time window.